Structural, magnetic and magnetotransport properties of $La_{0.7}Pb_{0.3}Mn_{0.9}TM_{0.1}O_3$ (TM = Fe, Co, Ni) CMR perovskites

2000 J. Phys.: Condens. Matter 12 10523

(http://iopscience.iop.org/0953-8984/12/50/313)

J. Phys.: Condens. Matter **12** (2000) 10523–10534. Printed in the UK PII: S0953-8984(00)15459-1

Structural, magnetic and magnetotransport properties of $La_{0.7}Pb_{0.3}Mn_{0.9}TM_{0.1}O_3$ (TM = Fe, Co, Ni) CMR perovskites

J Gutiérrez†, A Peña‡, J M Barandiarán†, J L Pizarro§, L Lezama‡, M Insausti‡ and T Rojo‡

† Departmento de Electricidad y Electrónica, Universidad del País del País Vasco/EHU, PO Box 644, E-48080 Bilbao, Spain

‡ Departmento de Química Inorgánica, Universidad del País del País Vasco/EHU, PO Box 644, E-48080 Bilbao, Spain

§ Departmento Mineralogía y Petrología, Universidad del País del País Vasco/EHU, PO Box 644, E-48080 Bilbao, Spain

Received 13 July 2000, in final form 3 October 2000

Abstract. Neutron-diffraction, magnetic and transport measurements have been used in order to study the structural and magnetic changes of the magnetoresistive $La_{0.7}Pb_{0.3}Mn_{0.9}TM_{0.1}O_3$ (TM = Fe, Co, Ni) perovskite-like compounds. Samples were prepared by the sol–gel low-temperature method. In all cases the exact stoichiometry is slightly different from the nominal one probably due to the presence of cation vacancies. All the phases exhibit ferromagnetic behaviour and magnetoresistance. No appreciable differences in the structure, as the TM^{3+} ion changes, have been observed. The magnetic moment and Curie temperature continuously decrease (with respect to the undoped composition) with the substitution of Mn atoms by Ni, Co or Fe, respectively. The magnetoresistance (MR $= \Delta R/R(0)$), under 0 and 6 T applied fields, has been measured reaching a magnitude of about 65% in the case of the 10% Fe doped sample. The obtained results can be interpreted in terms of ferro- or antiferromagnetic exchange competitions between Mn^{3+}–Mn^{4+} and TM^{3+}–Mn^{4+} pairs.

1. Introduction

The re-discovery of colossal magnetoresistance (CMR) in hole doped perovskites with formula $Ln^{3+}_{1-x}A^{2+}_xMnO_3$ (Ln = La, Sm, Nd, ...; A = Ca, Pb, Sr, ...) in the early 1990s gave rise to a new investigation subject of great interest, due to the fundamental physics involved in transport phenomena in ordered materials and also to their possible technological applications [1] such as magnetic heads. These manganites, on applying a magnetic field, exhibit a decrease of the resistance near their Curie temperature (T_C). The ferromagnetic properties of this type of compound were explained by means of the double exchange mechanism that involves Mn^{3+}–O–Mn^{4+} bonds [2]. The appearance of magnetoresistance [3] is related to the simultaneous presence of ferromagnetism and metallic state. These generic magnetic and transport properties in this type of doped manganites mainly arise from a strong on-site exchange interaction (Hund-rule couple $J \approx 2$–3 eV [4]) between the localized t_{2g} spins and itinerant e_g electrons [5].

An essential factor in order to understand the behaviour of these compounds is that the actual crystallographic structure presents a rhombohedral distortion of the classic cubic symmetry of the perovskite-like compounds [6], as neutron-diffraction studies have elucidated for the classical composition $La_{0.7}Ca_{0.3}MnO_3$ as well as for many other compositions.

0953-8984/00/5010523+12$30.00

In a similar way, the substitution of the Mn ions by other transition metal ions in perovskites of composition $La_{0.7}A_{0.3}Mn_{1-y}TM_y^{3+}O_3$ (TM = transition metal) gives rise also to changes in the Mn^{3+}:Mn^{4+} ratio, with important modifications in the magnetic and transport properties [7–11]. The $y = 0$ sample shows ferromagnetism and CMR. In this sense, the effect of different trivalent ions from the iron group (partially filled 3d shells) such as Fe^{3+} ($3d^5$), Co^{3+} ($3d^6$) or Ni^{3+} ($3d^7$) substitution in the Mn site is not yet well understood. For these cations, the Fermi level locates in the d band, and strong electron correlations must be expected in this band.

From previous studies, it is known that the effect of doping with transition metal ions is more drastic in the layered family of perovskites $R_{2-2x}M_{1+2x}Mn_2O_7$ (where R is a trivalent rare-earth element and M is a bivalent alkaline-earth metal) than in the $Ln_{1-x}A_xMnO_3$-type perovskite manganese oxides [12]. In fact, while a 20% Fe doping level is needed to suppress the ferromagnetic character of these latter compounds, the layered perovskite oxides show a more fragile ferromagnetic state that is suppressed with only a 7% Fe doping level.

We have shown, in a previous work [13], that iron enters as high-spin, $t_{2g}^3e_g^1$ (HS, $S = 5/2$) Fe^{3+} in the $La_{0.7}Pb_{0.3}Mn_{1-x}Fe_xO_3$ family of compositions because it is the most stable oxidation state for this cation, and its ionic radius is very similar to that of the Mn^{3+} ion. On the other hand, the spin state of the Co^{3+} ions depends on the temperature range, presenting a $t_{2g}^6e_g^0$ diamagnetic low-spin configuration at low temperatures (LS, $S = 0$) which changes above 35 K to a $t_{2g}^4e_g^2$ high-spin (HS, $S = 2$) state. The low-temperature spin state of the Co ion is due to the large crystal field, that stabilizes its low-spin configuration, which is energetically more favourable. However, both low- and high-spin states have a low energy difference ($\approx$0.03 eV) and so a transition between those states will appear due to thermal excitation. In the range 100–350 K both populations are stabilized in a ratio 50:50 in a dynamical equilibrium [14, 15]. Finally, the most stable Ni ion configurations are the high-spin Ni^{2+}, $t_{2g}^6e_g^2$ (HS, $S = 1$) and the low-spin state Ni^{3+}, $t_{2g}^6e_g^1$ (LS, $S = 1/2$). This last ion as well as Mn^{3+} ($t_{2g}^3e_g^1$) are Jahn–Teller ions with a single e_g electron with crystal degeneracy.

2. Experimental

Mixed oxides of nominal composition $La_{0.7}Pb_{0.3}(Mn_{0.9}TM_{0.1})O_3$ (TM = Fe, Co, Ni) were prepared by the sol–gel method with the required quantities of La_2O_3, $Pb(NO_3)_2$, $Mn(C_2H_3O_2)_2 \cdot 4H_2O$, $Fe(NO_3)_3 \cdot 9H_2O$, $Co(NO_3)_2 \cdot 6H_2O$ and $Ni(NO_3)_2 \cdot 6H_2O$ as the starting materials. Citric acid and ethylene glycol were used as gelling agents for the La and Mn ions in a nitrate solution. For these compositions the sol–gel fabrication process is the most adequate due to the high diffusion ability of the Pb ions. This method allows shorter reaction times and lower temperatures than the ceramic one.

After drying in a sand bath at 373 K for 24 h, the gel obtained was subjected to successive heat treatments at different temperatures, 773, 973 and 1073 K respectively, each of them for 10 h. In order to measure the electrical resistivities of the samples, the powder thus obtained was pelletized with a pressure of 3 tonnes cm^{-2} and sintered at 1173 K for 10 h in flowing oxygen.

The Mn^{3+}/Mn^{4+} content of each sample was determined by redox titration using an excess of $FeSO_4$ (0.025 M) solution and back-titration with $KMnO_4$(0.5 M). We have observed deviations from the theoretical stoichiometries that could be due to an excess in the oxygen concentration or more probably to the presence of cation vacancies [16]. The ratio Mn^{3+}:Mn^{4+} remains almost constant for the three samples, with a value 0.37:0.53.

The first crystallographic characterization of the phases of the samples was performed by x-ray powder diffraction analysis using STOE diffractometer equipped with a germanium

monochromator, working with Cu Kα_1 radiation. At room temperature, the diffraction maxima of the La phases were indexed in a rhombohedral space group ($R\bar{3}c$).

Magnetic and magnetoresistance measurements were conducted in a Quantum Design MPMS-7 SQUID magnetometer. The zero-field cooling (ZFC) and field cooling (FC) curves were performed under an applied field of 10 mT. $M(T)$ curves at 1 T applied field and hysteresis loops at 10 K and up to 7 T were also obtained. The resistance and magnetoresistance versus temperature measurements were taken by using a dc four-wire system with the current flowing parallel to the applied field. The pellets obtained from the synthesis procedure were cut in rectangular shape ($\approx$5 mm $\times$ 6 mm) and silver dag contacts were used. The irregularity of these contacts makes it difficult to give accurate values of the resistivity of the samples.

ESR spectra were recorded on a Bruker ESP 300 spectrometer, equipped with a standard Oxford low-temperature device, operating a X and Q bands. This apparatus was calibrated by NMR probe for the magnetic field, and by using a Hewlett–Packard 5352B microwave frequency counter for the resonant frequency in the cavity.

Neutron diffraction measurements were performed at the high-flux reactor at the Institut Laue–Langevin, Grenoble, France. For accurate refinements of the crystal and magnetic structures, measurements were carried out on D2B ($\lambda = 1.594$ Å), for the Fe doped composition. For tracing the temperature dependence of the structural and magnetic properties, instrument D1B, using a wavelength of 2.519 Å, was used. At this instrument, we studied the range $2\theta = 2$–90° at temperatures ranging from 1.8 to 300 K. The Rietveld analysis of the diffraction data was performed using the FULLPROF program [17]. The line shape of the diffraction peaks was generated by a pseudo-Voigt function, and the background interpolated between some fixed background points of the diagrams. The coherent neutron scattering lengths for La, Pb, Mn, Fe, Co, Ni and O were taken from [18]. In the final run the following parameters were refined: unit-cell parameters, zero-point, half-width, pseudo-Voigt and asymmetry parameters, scale factor, atomic coordinates and thermal isotropic factors. The occupancy factors of the La, Pb, Mn and TM atoms were also allowed to vary in the last steps of the refinements. Due to the high correlation between the thermal and occupancy factors, in some cases the refinements did not reach convergence. In these cases, the occupancy factors were fixed to the theoretical ones.

3. Results

3.1. Magnetic properties

Figure 1 shows the magnetic behaviour observed from ZFC and FC measurements for the three compositions studied in this work. From the ZFC curves we have determined the order temperature, T_C, as the temperature where the minimum of the $\mathrm{d}M/\mathrm{d}T$ derivative occurs. There is a remarkable similarity in the ZFC–FC curve behaviour for the samples containing Fe and Ni as doping elements, indicating that the magnetization processes involved at low applied field values are very similar: there is sharp increase in its value around T_C, and the obtained curves spilt just below that temperature. For lower temperatures, the magnetization slightly increases its magnitude, with the larger FC magnetization that reflects domain motion [19]. These samples exhibit the low-field magnetization behaviour of an ordinary ferromagnet.

For the Co containing sample, the ZFC measured curve shows a peak and below that peak the magnetization decreases with the decrease of the temperature. In principle, this behaviour is classical of cluster or spin glass systems. However, that decrease of the magnetization could be also due to the competition between the high-spin and low-spin configuration states of the cobalt ion, as temperature decreases.

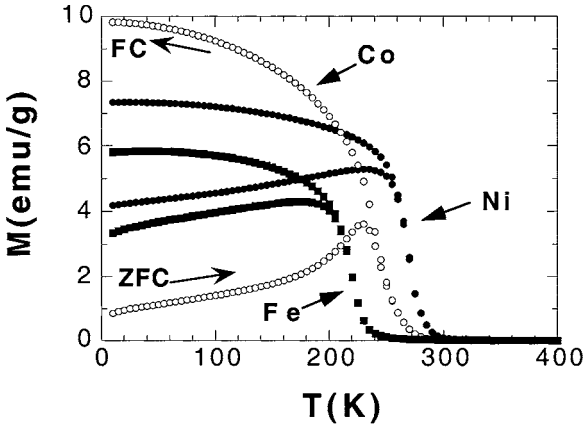

Figure 1. Zero-field cooling (ZFC, increasing temperature arrow) and field cooling (FC, decreasing temperature arrow) curves measured for the three samples studied in this work.

Hysteresis loops have been also measured at 10 K and up to 7 T. There are several interesting features to be analysed (see figure 2): the samples corresponding to Fe and Ni containing compositions behave as usual ferromagnetic samples, reaching the magnetic saturation already for applied fields of 3 T. However, this is not the case of the Co containing composition: even it if shows a normal ferromagnetic behaviour, the arrival at magnetic saturation occurs at a slower rate. In addition to this fact, a much higher value of the coercive field ($H_c^{Co} = 98$ kA m^{-1}) has been measured for this sample, in comparison with the Fe and Ni doped ones ($H_c^{Fe} \approx H_c^{Ni} \approx 5.6$ kA m^{-1}). This difference in the magnitude of the coercive field measured at low temperature can be understood as arising from the strong anisotropic nature of the Co ion [20].

The X band ESR spectra of the samples have been recorded at room temperature (see figure 3), that is above the Curie temperature of all the samples. As a first consequence, all signals should be Lorentzian-like ones, indicating insulating behaviour. However, the curve corresponding to the Ni doped composition shows also clearly Dysonnian-like behaviour (conducting) influence, as it must be the case since room temperature is not very far from the Curie one.

We have observed only a small broadening of the resonance line when Mn atoms are substituted by Ni. This effect is mainly due to the reduction of the Curie temperature and implies that the g-value of the Ni spin system is close to $g = 2$. In octahedral coordination, this is the case of high-spin Ni^{2+} and low-spin Ni^{3+} ions. However, while low-spin Ni^{3+} systems give rise usually to narrow ESR signals at room temperature, high-spin Ni^{2+} systems are not easily observed due to a strong single-ion zero-field splitting. In our case, the reduction in the Curie temperature together with the obtained resonance line shape for the Ni doped composition, allow us to assume that only low-spin Ni^{3+} ion is present.

3.2. Magnetoresistance behaviour

The room-temperature estimated values of the resistivity are about 0.258, 0.098 and 0.071 (Ω cm) for the samples doped with Fe, Co and Ni, respectively. As expected, the Ni containing sample exhibits the lowest resistivity value [21]. The measured value for the undoped $La_{0.7}Pb_{0.3}MnO_3$ sample is about 0.024 (Ω cm) [8].

The temperature dependence of the resistivity of materials such as the hole-doped perovskites has been very difficult to model due to the combined effects of many types of

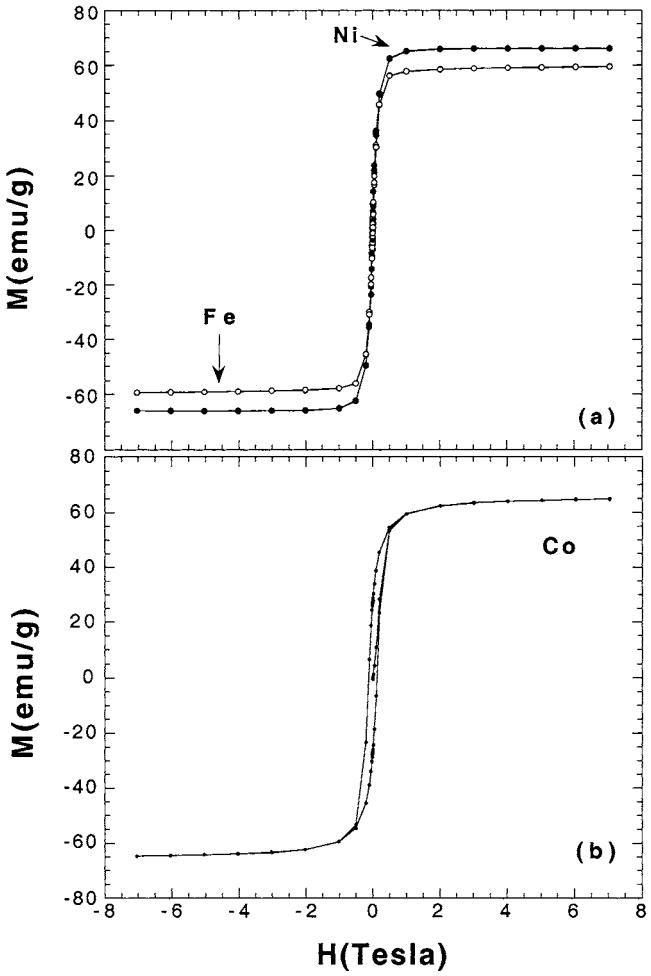

Figure 2. Hysteresis loops measured at 10 K for the: (a) Fe and Ni and (b) Co 10% doped compositions.

interaction: band structure, Coulomb interactions, grain boundaries, oxygen content and many others. For the compositions of our study, at low temperatures where the $M(T)$ behaviour indicates that the local ferromagnetic order is almost complete, the resistance versus temperature behaviour fits well to the expression

$$R(T) = R_0 + R_1 T^{2.5}. \tag{1}$$

This $R_1 T^{2.5}$ term is an empirical fit that has been interpreted to arise from a combination of electron–electron and electron–magnon scattering [22]. For $T > T_C$, our zero-field resistance data fit well to the equation

$$R(T) = R_0 \exp\left(\frac{T_0}{T}\right)^{1/2} \tag{2}$$

which corresponds to the Mott variable range hopping mechanism (VRH) [23], when the carriers are localized near the Fermi energy, as it is in our case. Efros and Shklovii [24] showed that the exponent $n = 1/2$ is directly related to a form of hopping favoured by the Coulomb

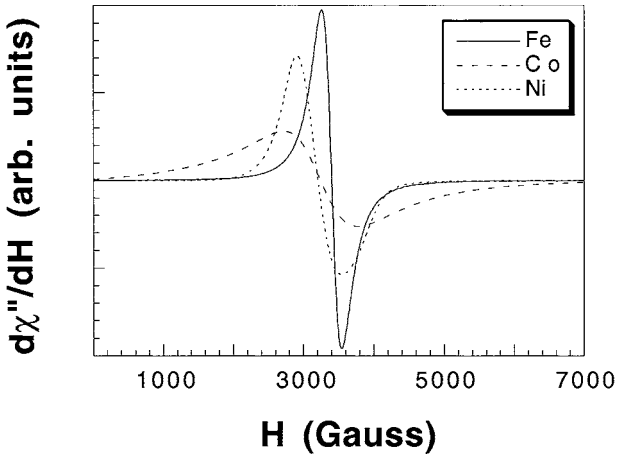

Figure 3. X band ESR spectra obtained at room temperature.

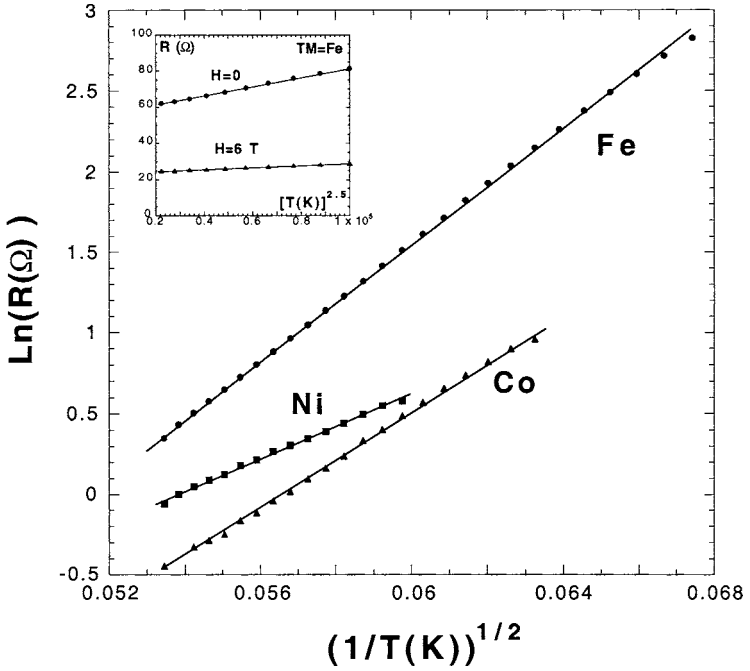

Figure 4. High-temperature $\ln(R)$ versus $T^{-1/2}$ dependence for all the samples. The onset shows the obtained low-temperature $R(T^{2.5})$ linear dependence, for the Fe doped sample.

repulsion between carriers, since the localized states are not very effective in screening the long-range part of the Coulomb interaction. Its most important effect is the existence of the Coulomb gap [25, 26], that basically reflects the difference between the minimum energies of adding an electron and subtracting one from the system, without disturbing the other charges.

The $\ln R$ versus $T^{-1/2}$ dependence is shown in figure 4. We have found values of $T_0 = 3.2\times10^4$ K, 2.22×10^4 K and 1×10^4 K for the corresponding Fe, Co and Ni compositions, that lead directly to Coulomb gap values of 2.8 eV, 1.9 eV and 0.9 eV, respectively. In the

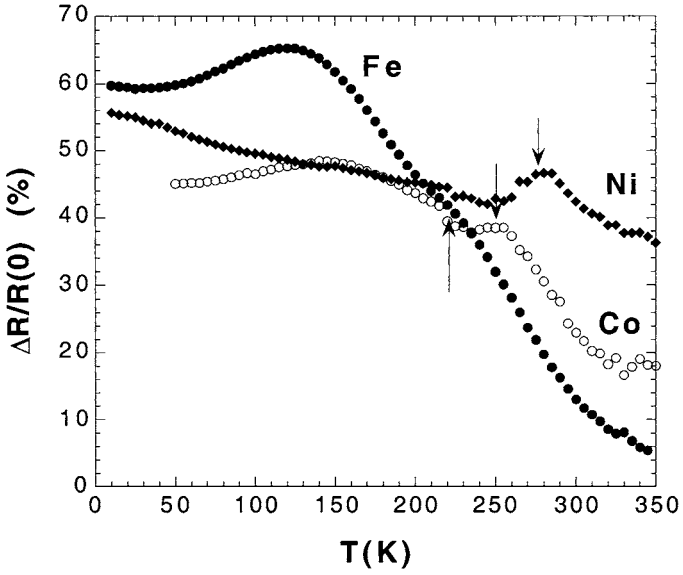

Figure 5. Magnetoresistance behaviour versus temperature. Arrows indicate the Curie temperature for each sample.

range of temperatures studied, these energy values are bigger than k_BT, this fact being in good concordance with our assumption of the VRH mechanism. Also, the lowest value of the Coulomb gap has been obtained for the 10% Ni doped sample, that agrees with the observed better conductive behaviour.

It has to be noticed that this calculus with $n = 1/4$ (that corresponds also to the VRH equation of the Mott type, but when the thermal hopping energy is large compared with the Coulomb gap) gives a good fit of the data. However, the obtained values of R_0 and T_0 are unphysical.

The change of the resistance measured under zero and 6 T applied fields, as a function of temperature, has been also determined. In absence of external field a sharp resistance maximum, characteristic of a semiconductor–metal transition, has been found for all compositions. The decrease of the resistance value observed when a 6 T external field is applied allows us to use the definition of the relative negative magnetoresistance as $[R(6\,\mathrm{T}) - R(0\,\mathrm{T})]/R(0\,\mathrm{T})$ [3]. The measured magnetoresistances for all samples are shown in figure 5. While the sample doped with Fe shows a shoulder, Co and Ni doped samples exhibit a small peak, all behaviours close to the Curie temperature of each composition. This fact has been explained as indicating different contributions to the magnetoresistance: an intrinsic (intragrain) one near the Curie temperature, due to the fact that the granular perovskite behaves in the ferromagnetic state as a granular ferromagnet [27, 28]. On the other hand, and specially for the Fe and Co doped compositions, there is a maximum in the magnetoresistance at a temperature well below T_C, that has been interpreted as the contribution of the intergrain magnetoresistance (due to the difference in the magnetic order between surface and core of the perovskite grains) [29].

3.3. Neutron-diffraction study

The crystal structure of this family of compounds has been analysed in the trigonal space group ($R\bar{3}c$), hexagonal setting ($Z = 6$), using the D2B neutron powder diffraction data obtained at

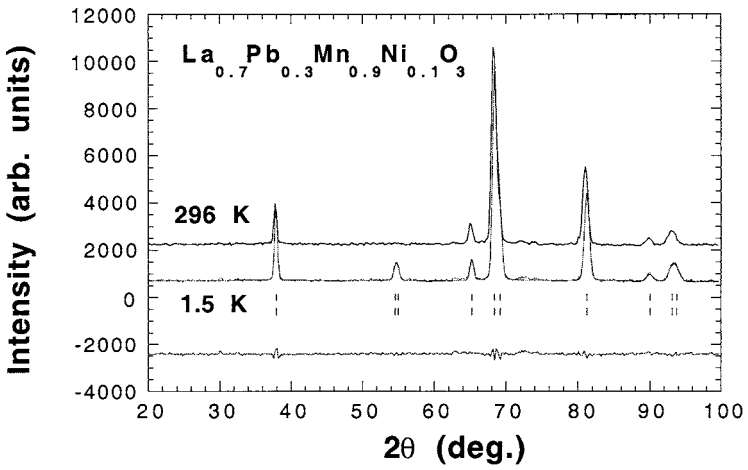

Figure 6. Rietveld refinement of the $La_{0.7}Pb_{0.3}Mn_{0.9}Ni_{0.1}O_3$ neutron-diffraction spectrum obtained at 1.5 K and room temperature (the intensity is in arbitrary units). The difference between measured and calculated data is plotted below. The second series of tick marks indicates the magnetic contribution.

room temperature. The La atoms are at (0, 0, 1/4) positions, Mn at (0, 0, 0) and O at (x, 0, 1/4). The Fe, Co or Ni atom was placed at the Mn site, with the corresponding occupation factor for both ions. The Fe containing sample shows weak extra lines corresponding to a small amount of Mn_2O_3 as impurity (<3%) (Bixbyite, ASTM number 41-1442). This impurity arises during the sample fabrication process, when the solid reaction, at high temperature (between 550 and 900 °C) in the presence of air, takes place. For this composition, Mn_2O_3 was included in the refinements as second phase. Figure 6 shows the refinement of the $La_{0.7}Pb_{0.3}Mn_{0.9}Ni_{0.1}O_3$ neutron-diffraction spectra (from the D1B instrument) obtained at 1.5 K and also at room temperature. The final atomic parameters after the refinements are shown in table 2.

The substitution of Mn by one of these transition metal ions produces only minor distortion in the MnO_6 octahedra, the O–Mn–O and Mn–O–Mn angles remaining rather constant. Furthermore, the tolerance factor (t) of the perovskite structure, $t = (d_{La-O}/2(d_{Mn-O})$, with d_{La-O} and d_{Mn-O} the La–O and Mn–O bond distances, remains constant ($t = 0.994$) for the three different compositions. The unit-cell volume and the Mn/TM–O distances slightly decrease as Mn is substituted by Fe, Co or Ni, respectively. These geometrical characteristics are in good agreement with the slightly smaller size of Fe^{3+}, Co^{3+} and Ni^{3+} ions with respect to the Mn^{3+} ions.

The thermal evolution of the diffraction patterns for all the samples was recorded at the D1B instrument. Two reflections with magnetic contribution appear at low temperatures, with the same d values for all compositions. This feature is indicative of an equivalent magnetic structure for all compounds. That is, the magnetic order does not change its structure when including 10% of TM in the La phases. Furthermore, all magnetic reflections can be indexed with the same cell as the nuclear one, indicating an equivalent type of ferromagnetic structure. The thermal evolution of the intensity of the overlapped (110)+(104) peaks with magnetic contribution (at $2\theta \approx 55^\circ$) is shown in figure 7. This magnetic contribution appears at about 230 K, 290 K and 280 K for the Fe, Co and Ni containing samples, respectively. The Rietveld refinement of the data recorded far below these temperatures was performed taking into account the magnetic contribution as a second phase. The best solution was obtained with a collinear magnetic structure in which the magnetic moment of the Mn ion is placed into the (110)

Table 1. Values of the order temperature (T_C) magnetic moment in the ordered state obtained from magnetic measurements (μ) and neutron diffraction experiments (μ^*), and transition temperature in the resistance behaviour (T_{SC-M}).

TM	T_C (K)	μ (μ_B)	μ^* (μ_B)	T_{SC-M} (K)
Fe	215	2.79	2.10	120
Co	240	3.05	2.74	125
Ni	265	3.11	2.62	175

Table 2. Rietveld refinement results for neutron-diffraction pattern of the $La_{0.7}Pb_{0.3}Mn_{0.9}TM_{0.1}O_3$ compositions.

Sample	TM = Fe	TM = Co	TM = Ni
T (K)	270	296	296
a (Å)	5.5235(1)	5.496(2)	5.492(1)
c (Å)	13.398(1)	13.346(4)	13.331(3)
V (Å^3)	353.99(1)	349.1(2)	348.2(1)
t	0.994	0.993	0.994
La B (Å^2)/F_{occ}	0.57(3)/0.7	0.247(3)/0.7	0.9(4)/0.7
Pb B (Å^2)/F_{occ}	0.57(3)/0.3	0.247(3)/0.3	0.9(4)/0.3
Mn B (Å^2)/F_{occ}	0.79(8)/0.9	0.247(3)/0.9	0.9(4)/0.9
TM B (Å^2)/F_{occ}	0.79(8)/0.1	0.247(3)/0.1	0.9(4)/0.1
O x	0.4569(1)	0.4592(1)	0.4574(1)
O B (Å^2)/F_{occ}	1.11(2)/3.0	1.4(4)/0.531	1.6(4)/0.532
Mn/TM–O (Å)	1.9610 × 6	1.9505 × 6	1.9487 × 6
LA/Pb–O (Å)	2.5236 × 3	2.5241 × 3	2.5212 × 3
	2.7541 × 6	2.7413 × 6	2.7386 × 6
	3.0000 × 3	2.9720 × 3	2.9703 × 3
⟨La/Pb–O⟩ (Å)	2.758	2.7447	2.7422
Mn/TM–O–Mn/TM (°)	166.06	166.81	166.77
O–Mn/TM–O (°)	90.79	90.71	90.72
Mn_2O_3 (%)	2.57		
Discrepancy factors			
R_p (%)	4.82	3.41	3.15
R_{wp} (%)	6.13	4.82	4.33
R_e (%)	3.09	3.01	3.24
χ^2	3.92	2.57	1.79
R_B (%)	3.89	3.70	2.62

crystallographic plane, in the hexagonal setting (perpendicular to the [111] direction of the perovskite cubic cell).

4. Discussion and conclusions

The results obtained from magnetic measurements are summarized in table 1. If we compare these values with those obtained for the $La_{0.7}Pb_{0.3}MnO_3$ composition [13] (3.28 μ_B/atom and $T_C = 345$ K), it can be inferred that the effect of the substitution of 10% of Mn atoms by TM ones is a decrease in the order temperature and the magnetic moment measured at 10 K and 7 T applied field. If titration data for the Mn^{3+}/Mn^{4+} content of our samples are reliable, under the assumption that the compounds are $La^{3+}_{0.7}Pb^{2+}_{0.3}Mn^{3+}_{0.37}Mn^{4+}_{0.53}TM^{3+}_{0.1}O_3$, we are led to

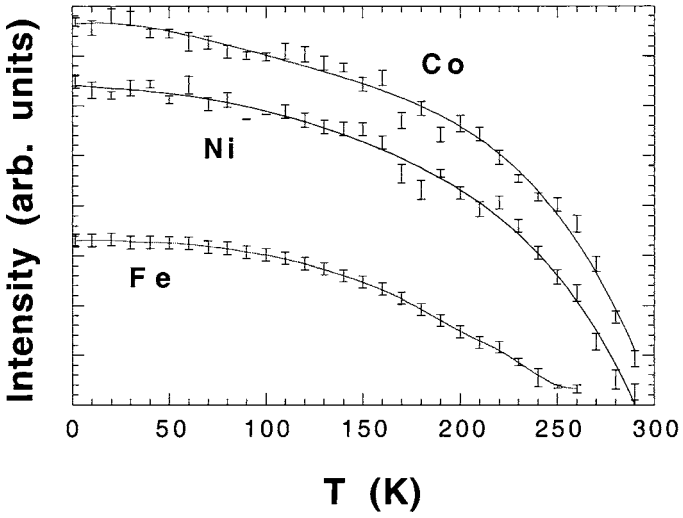

Figure 7. Temperature dependence of the magnetic moment obtained from neutron-diffraction experiments.

a low-temperature ferromagnetic moment of

$$M = [4 \times 0.37 + 3 \times 0.53 + 0.1\ \mu_{TM}]\mu_B = [3.07 + 0.1\ \mu_{TM}]\mu_B. \tag{3}$$

Compared with the obtained experimental values, this expression immediately indicates different kinds of interaction of the TM ions with their neighbouring Mn ions. In the case of the Fe doped sample, a simple consideration of antiferromagnetic coupling of all $Fe^{3+}(\mu = 5\ \mu_B)$ ions with respect to the Mn ones gives directly an expected value for the moment of $3.07 - 0.1 \times 5 = 2.57\ \mu_B$. If we consider the case of the Co doped sample, at the low temperature we are dealing with, the ion will be present in its diamagnetic low-spin state. That is, not magnetic contribution from Co can be expected for this composition. As a result, the calculated value of the expected moment should be $3.07\ \mu_B$. Finally, from EPR experiments the presence of low-spin Ni^{3+} ions was detected in the sample containing Ni as doping element. Other authors have already reported that the Ni^{3+}–O–Mn^{3+} and Ni^{3+}–Mn^{4+}–Ni^{3+} interactions appear to be ferromagnetic [30]. In fact, the single e_g electron of this ion favours the electron hopping with the Mn, and so the double exchange and ferromagnetic character for this composition. It we assume that only Ni^{3+} (LS) is present in our sample, with a magnetic contribution of $1\ \mu_B$, a simple calculation gives immediately $3.07+0.1 \times 1 = 3.17\ \mu_B$ as the expected value of the low-temperature magnetic moment. That is, there is a good agreement between expected values of the low-temperatures spontaneous magnetic moment and measured ones, for the three studied samples.

Neutron-diffraction data corroborate these assumptions: if we consider the values of the volume of the unit cell obtained at high temperature (see table 2), we can observe that they are very close for the Co and Ni containing compositions. Taking into account the different ionic radii of the transition metal ions [31], these close volume values immediately correlate with the supposition that at those high temperatures there is a mixture of Co^{3+}(HS) and Co^{3+}(LS) (that gives an averaged ionic radius $\langle r_{Co} \rangle = 0.7161$ Å) and only Ni^{3+}(LS) (with $\langle r_{Ni} \rangle = 0.7155$ Å), for the two samples.

The different ferro- or antiferromagnetic interactions appearing as the doping TM ion changes have been also corroborated by the neutron diffraction experimental data refinements.

Those fits were performed taking into account the previous considerations made when comparing the low magnetic moment value of each composition. That is, we have to consider first the Fe to enter completely with antiferromagnetic coupling with respect to Mn; for the Co, at low temperature we have considered that it does not participate in the magnetic moment in the refinement of the low-temperature neutron-diffraction data. Finally, we have supposed a ferromagnetic contribution in the case of the Ni doped sample neutron-diffraction data refinement, since we assumed that only low-spin Ni^{3+} appears in its composition. In all cases the respective relative occupancy factor was taken into account.

Following these considerations and from careful refinement of the low-temperature (1.5 K) spectra, we have obtained estimated values of the magnetic moment of 2.1 μ_B, 2.74 μ_B and 2.62 μ_B, for the Fe, Co and Ni doped samples, respectively. These values are lower than those obtained from magnetic methods. In any case, the differences between these estimated values clearly confirm the different kinds of magnetic interaction among the different samples.

In the light of our experimental work, we can conclude that the transition metal doped $La_{0.7}Pb_{0.3}Mn_{0.9}TM_{0.1}O_3$ perovskite-like compounds show low distortion in the structure as the TM changes. For this precise doping level (10% TM) the ferromagnetic character of all samples still remains and this is mainly due to the double exchange mechanism that arises from the almost constant value of the ratio Mn^{3+}:Mn^{4+}. The measured low-temperature saturation magnetic moments are mainly due to the different magnetic moment of these TM^{3+} ions and the different kinds of magnetic interaction that appear as the TM ion changes. In spite of these different interactions, the ferromagnetic character of all compositions remains unchanged. With respect to the undoped composition, the Curie temperature decreases continuously as Ni, Co or Fe ions enter respectively into the composition. All studied samples show magnetoresistance, with maximum magnitudes of 65% and 48% for the samples doped with Fe and Co, respectively, and ranging around 40–50% for the Ni containing sample.

Acknowledgments

We would like to thank the Spanish partnership of CRG-D1B at the Institute Laue–Langevin, Grenoble, France. We would also like to thank the local contact at this institution, Javier Campo, for his help.

This work was partially supported by the Spanish CICyT under project MAT1999-0667-C04-02 and the University of the Basque Country (UPV/EHU) under project UPV224.310-G22/99.

References

[1] Prinz G A 1995 *Phys. Today* **48** 58
[2] Zener C 1951 *Phys. Rev.* **82** 403
[3] Chahara K, Ohno T, Kasai M and Kozono K 1993 *Appl. Phys. Lett.* **63** 1990
[4] Moritomo Y, Machida A, Matsuda K, Ichida M and Nakamura A 1997 *Phys. Rev.* B **56** 5088
[5] Anderson P W and Hasewaga H 1995 *Phys. Rev.* **100** 675
[6] Radaelli P G, Marezio M, Hwang H Y, Cheong S W and Batlogg B 1996 *Phys. Rev.* B **54** 8992
[7] Righi L, Gorria P, Insausti M, Gutiérrez J, Barandiarán J M 1997 *J. Appl. Phys.* **81** 5767
[8] Gutiérrez J, Barandiaŕan J M, Insausti M, Lezama L, Peña A, Blanco J J and Rojo T 1998 *J. Appl. Phys.* **83** 7171
[9] Pissas M, Kallias G, Devlin E, Simopoulos A and Niarchos D 1997 *J. Appl. Phys.* **81** 5770
[10] Ahn K H, Wu X W, Liu K and Chien C L 1996 *Phys. Rev.* B **54** 15 299
[11] Ghosh K, Ogale S B, Ramesh R, Greene R L, Venkatesan T, Gapchup K M, Bathe R and Patil S I 1999 *Phys. Rev.* B **59** 533
[12] Zhang J, Yan Q, Wang F, Yuan P and Zhang P 2000 *J. Phys.: Condens. Matter* **12** 1981 and references therein

[13] Gutiérrez J, Peña A, Barandiarán J M, Pizarro J L, Hernández T, Lezama L, Insausti M and Rojo T 2000 *Phys. Rev.* B **61** 9028
[14] Mira J, Rivas J, Sánchez R D, Señarís-Rodríguez M A, Fiorani D, Rinaldi D and Caciuffo R 1997 *J. Appl. Phys.* **81** 5753
[15] Gayathri N, Raychaudhuri A K, Tiwary S K, Gundakaram R, Arulraj A and Rao C N R 1997 *Phys. Rev.* B **56** 1345
[16] Rao C N R, Cheetham A K and Mahesh R 1996 *Chem. Mater.* **8** 2421
[17] Rodríguez-Carvajal 1990 *'FULLPROF' Program, Rietveld Pattern Matching Analysis of Powder Patterns'* ILL, Grenoble
[18] Sears V F 1984 Thermal neutron scattering lengths and cross sections for condensed matter research *Chalk River Nuclear Laboratory Internal Report* AECL-8490
[19] Ju H L and Sohn H 1997 *J. Magn. Magn. Mater.* **167** 200 and references therein
[20] Carlin R L 1986 *Magnetochemistry* (New York: Springer)
[21] Gayathri N, Raychaudhuri A K, Xu X Q, Peng J L and Green R L 1999 *J. Phys.: Condens. Matter* **11** 2901 and references therein
[22] Schiffer P, Ramírez A P, Bao W and Cheong S W 1995 *Phys. Rev. Lett.* **75** 3336
[23] Mott N F 1968 *J. Non Cryst. Solids* **1** 1
[24] Efros A L and Shklovskii B L 1975 *J. Phys. C: Solid State Phys.* **8** L49
[25] Pollack M 1970 *Discuss. Faraday Soc.* **50** 13
[26] Srinivasan G 1971 *Phys. Rev.* B **4** 2581
[27] Jin S, Tiefel T H, McCormack M, Fastnacht R A, Ramesh R and Chen L H 1994 *Science* **264** 413
[28] von Helmollt R 1975 *Phys. Rev. Lett.* A **54** 225
[29] Zhang N, Ding W, Zhong W, Xing D and Du Y 1997 *Phys. Rev.* B **56** 8138
[30] Goodenough J B, Wold A, Arnott R J and Menyuk N 1961 *Phys. Rev.* **124** 373
[31] Shannon R D 1976 *Acta Crystallogr.* A **32** 751